Available online at www.sciencedirect.com
SCIENCE DIRECT®
Catalysis Today 93–95 (2004) 45–53
CATALYSIS TODAY
www.elsevier.com/locate/cattod

Ceria-based fluorite-like oxide solid solutions as catalysts of methane selective oxidation into syngas by the lattice oxygen: synthesis, characterization and performance

V.A. Sadykov[a,*], T.G. Kuznetsova[a], G.M. Alikina[a], Y.V. Frolova[a], A.I. Lukashevich[a], Y.V. Potapova[a], V.S. Muzykantov[a], V.A. Rogov[a], V.V. Kriventsov[a], D.I. Kochubei[a], E.M. Moroz[a], D.I. Zyuzin[a], V.I. Zaikovskii[a], V.N. Kolomiichuk[a], E.A. Paukshtis[a], E.B. Burgina[a], V.V. Zyryanov[b], N.F. Uvarov[b], S. Neophytides[c], E. Kemnitz[d]

[a] *Boreskov Institute of Catalysis SB RAS, Novosibirsk, Russia*
[b] *Institute of Solid State Chemistry SB RAS Novosibirsk, Russia*
[c] *Institute of Chemical Engineering and High Temperature Processes, Patras, Greece Russia*
[d] *Institute for Chemistry, Humboldt University, Berlin, Germany*

Available online 15 July 2004

Abstract

Polymerized precursor route [M.P. Pechini, US Patent 3, 330 (1967) 697] was applied for synthesis of dispersed ceria-based solid solutions $Ce_{1-x}Me_x^{3+}O_{3-y}$ (Me^{3+}= Sm^{3+} or Bi^{3+}, x up to 0.5). The surface properties of those samples were modified by supporting Pt. Their bulk and surface structural features were characterized by using XRD, TEM, EXAFS, X-ray wide angle scattering (RED), UV–vis, Raman, FTIRS of lattice modes and adsorbed CO. To elucidate factors controlling the surface/bulk oxygen mobility and reactivity, these results were compared with the data of‘ the oxygen isotope exchange and/or H_2/CH_4 temperature-programmed reduction (TPR). Single-phase fluorite-like solid solutions with a nanodomain microstructure are characterized by distortion of the coordination polyhedra caused by dopants followed by the lattice local rearrangement into that of a lower symmetry at a high dopant content. The highest performance in methane selective oxidation into syngas by the lattice oxygen is found for samples where isolated oxygen vacancies dominate. Earlier studied Pt/Ce–Zr–La–O system [Stud. Surf. Sci. Catal. 143 (2002) 659; T.G. Kuznetsova, V.A. Sadykov, S.A. Veniaminov, G.M. Alikina, E.A. Paukshtis, Ya.N. Kulikova, E.M. Moroz, E.B. Burgina, V.A. Rogov, V.N. Kolomiichuk, V.V. Kriventsov, D.I. Kochubei, O.N. Martyanov, V.F. Yudanov, I.S. Abornev, S. Neophytides, ISO22, Europacat VI, September 2003, Innsbruck, Austria] has a lower oxygen mobility, is less stable in redox cycles and less selective for syngas. Bi–Ce–O system mainly combusts methane and is irreversibly decomposed by deep reduction due to metallic Bi evaporation.

Keywords: Ceria doped by Sm or Bi; Sructural and surface properties; XRD; TEM; EXAFS; RED; UV–vis; Raman; FTIRS; Surface/lattice oxygen mobility and reactivity; Methane selective oxidation into syngas

1. Introduction

Catalytic oxidation of methane (natural gas) into syngas by oxygen transferred through the membranes comprised of complex oxides with mixed ionic–electronic conductivity is now considered as a viable option in the natural gas conversion technologies including such application as hydrogen generation for fuel cells [4]. Ceria modified by low-valence cations (Sm, Bi etc.) possess a good ionic conductivity, while electronic conductivity can be generated either by forming nanocomposites with precious metals (Pt, Ag etc.) or through a partial reduction of those mixed oxides. For the side of membrane contacting with methane, the rate and selectivity of methane transformation into syngas and/or combustion products is expected to depend upon the surface oxygen bonding strength and mobility determined in turn by the mixed oxide chemical composition and real structure. Moreover, specific activation of methane on the metallic components (Pt etc.) could be important as well. However, this aspect of the catalytic oxygen conducting membranes design has not yet been properly addressed. It is also of primary importance for design of mixed oxide catalysts able to convert methane into syngas by the lattice oxygen

* Corresponding author. Tel.: +7 3832 343763; fax: +7 3832 343056.
E-mail address: sadykov@catalysis.nsk.su (V.A. Sadykov).

0920-5861/$ – see front matter © 2004 Elsevier B.V. All rights reserved.
doi:10.1016/j.cattod.2004.05.016

in redox cycles (with reoxidation of reduced systems by air or even by water or carbon dioxide) [5] or by the gas-phase oxygen at short contact times on monoliths [6].

This paper presents results of work aimed at design and characterization of catalysts for those processes comprised of ceria modified by Sm or Bi and promoted by Pt. The main idea is to enhance the oxygen mobility in the lattice of ceria by incorporating Sm^{3+} and Bi^{3+} cations (up to 50 at.%) while increasing the rate of methane dissociation by supporting Pt. For comparison, some results for earlier studied Pt/Ce–Zr–La–O system [2,3] are considered as well.

2. Experimental

Dispersed samples of ceria-based solid solutions were prepared by the complex polymerized method as in [1–3] and annealed at 500–700 °C. Pt (1.4 wt.%) was supported by the incipient wetness impregnation from the water solutions of H_2PtCl_6.

Electron microscopic data were obtained with a JEM-2010 microscope. The resolution limit was about 0.14 nm, the accelerating potential 200 kV. Specimens were deposited onto a holly-carbon film supported on a copper grid from the ethanol slurry.

The X-ray phase analysis of samples was carried out using a HZG-4C diffractometer (Cu Kα radiation and a flat monochromator) in the range of 2θ angles equal to 1–70°. The unit cell parameter of doped ceria samples was determined from the position of 3 1 1 diffraction peak. To obtain the curves of the electronic density radial distribution (RED), synchrotron radiation with $\lambda = 0.703$ Å (Siberian Synchrotron Radiation Center) was applied for measurements in the 2θ range 5–135° with a step of 0.1° [8].

Infra-red spectra of samples in the 220–4000 cm^{-1} range were registered using a BOMEM M spectrometer.

The Raman scattering measurements were carried out using 100/S-Bruker Raman Fourier Spectrometer. The 1.06 mm line of an Nd-YAG laser was used for excitation, an output laser power varied from 50 to 200 mW.

UV–vis spectra were recorded using a Shimadzu 8300 spectrometer equipped with a diffuse scattering DRS 8000 cell.

The surface properties were probed by the IR spectroscopy of adsorbed CO test molecule (a Fourier-transform IFS 113 V Bruker spectrometer) [7,8].

The EXAFS spectra of the Ce-L3 and Zr–K edges for all the samples studied were obtained at the EXAFS Station of Siberian Synchrotron Radiation Center. The radial distribution function (RDF) was calculated from the EXAFS spectra in $k^3\chi(K)$ as modulus of Fourier-transform [7,8].

BET specific surface area (S_{sp}, m^2/g) was determined from the data on the thermal Ar desorption.

Oxygen mobility up to 700 °C was estimated by using isotope exchange both in dynamic and isothermal conditions [9], while its reactivity was characterized by temperature-programmed reduction (temperature ramp 10 grad/min from 25 up to 880 °C) with H_2 (1% in Ar) or methane (1% in He). H_2, CH_4, CO and CO_2 were continuously monitored by using on-line IR absorbance gas analyzer PEM-2M, TCD and an electrochemical sensor with the data acquisition and processing through a PC.

3. Results and discussion

3.1. Structural properties

For both methods of synthesis, in all range of the dopant content, no traces of admixed phases either crystalline or amorphous were revealed, and the lattice parameter increases continuously with x, thus confirming formation of a single-phase fluorite-like solid solution (Fig. 1). For Bi-doped ceria, homogeneity of the solid solution up to $x = 0.5$ was earlier achieved only by using time-consuming hydrothermal treatment of sols precipitated by NaOH [10]. However, when NH_4OH was used as sol precipitating agent, the Bi solubility in ceria was found to be restricted to 20 at.% [11].

The specific surface area of samples doped by Bi or Sm and calcined at 500 °C reaches up to 100 m^2/g, thus demonstrating their good dispersion. For both systems, X-ray particle sizes tend to decline with x (up to a certain limit for Bi-doped samples). This implies that Me^{3+} dopants hinder sintering of domains via segregation at their boundaries, as was shown to be a general phenomenon for doped ceria samples [12]. These domains are in the nanosize range evidencing developed domain boundaries network. Smaller domain sizes for Bi-doped samples suggest a higher tendency for the Bi segregation at boundaries, which is explained by a bigger size of Bi^{3+} cation (1.31 Å) [10] versus Sm^{3+} (1.08 Å) and Ce^{4+} (1.11 Å) cations [13]. However, progressive enrichment of domain boundaries by Bi as its content increases makes their structure similar to that of Bi_2O_3 with a higher oxygen mobility [13] and low (825 °C) melting temperature, hence, a higher ability to sintering. As the result, at $x > 0.2$,

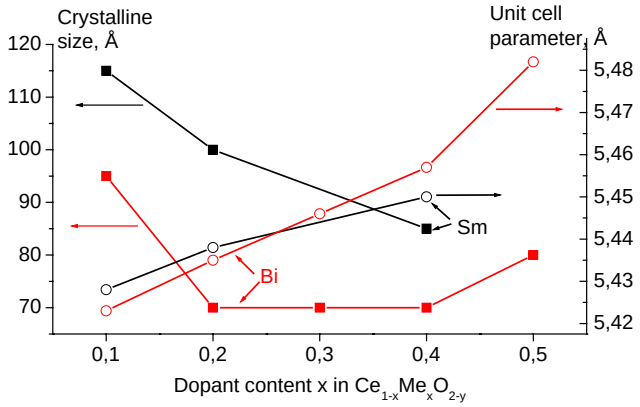

Fig. 1. X-ray particle sizes and unit cell parameters for ceria-based fluorite-like solid solutions versus dopant content.

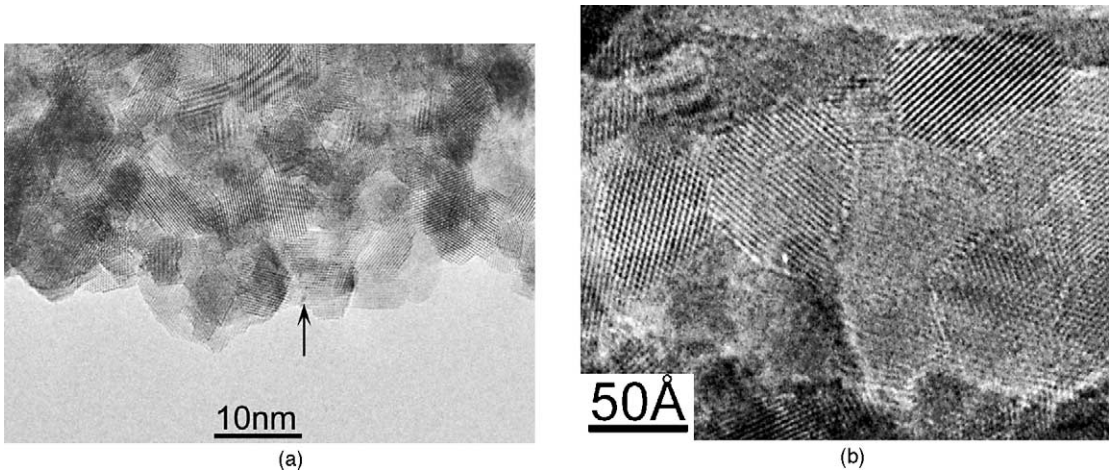

Fig. 2. Typical high-resolution TEM images of particles of fluorite-like ceria doped samples: (a) Pt/$Ce_{0.85}Sm_{0.15}O_{2-y}$; (b) $Ce_{0.8}Bi_{0.2}O_{2-y}$. A small Pt cluster located at the surface step of $Ce_{0.85}Sm_{0.15}O_{2-y}$ particle is arrowed.

domain sizes in Bi-doped samples first stabilize and then increase at the highest Bi content.

TEM data (Fig. 2) confirm microdomain type of particles with a good domain crystallinity (lattice planes are resolved) and a high density of rather disordered domain boundaries. These boundaries are known to affect the oxygen mobility in the lattice serving either as channels or barriers for oxygen anion diffusion in the lattice [14,15]. For Bi-doped samples, a strong variation of the image contrast within a domain implies a non-uniform spatial Bi distribution causing a structure rearrangement, which is also of significance for the oxygen mobility. For oxidized samples, supported Pt particles are practically not visible, which implies their high dispersion and/or deep oxidation. A small cluster can be visible at the edge of $Ce_{0.8}Sm_{0.2}O_{3-y}$ particle near the surface step (Fig. 2a, arrowed).

Analysis of X-ray radial electronic distribution density curves (not shown here for brevity) revealed that for both systems at a low dopant content, the metal-oxygen coordination number is decreased as compared with that for the ideal ceria structure (CN = 8) (see Table 1 for Ce–Sm–O system).

Since this method is not sensitive to the nature of a scattering element [8], and at a low Sm content the intensity of corresponding peak is determined mainly by Ce cations, this result implies that anion vacancies are located in the coordination sphere of Ce cation. This conclusion agrees with the EXAFS results of Yamazaki et al. [16] for ceria doped with lanthanides. However, disordering of the cation coordination sphere and its deformation should also be taken into account. Indeed, at the highest doping level this distance is split into two indicating a strong rearrangement of the structure making it locally tetragonal. The increase of the integral coordination number suggests that such a rearrangement removes isolated anion vacancies from the coordination sphere of cations. Modeling of RED curves proved that all these features could not be explained by appearance of clusters with samaria structure [17].

Table 1
Distances and coordination numbers for the first Me–O shell in Ce–Sm–O system calcined at 500 °C

Sm content (x)	First Me–O coordination sphere	
	Distance (Å)	Coordination number
0.1	2.35	6.2
0.2	2.35	5.5
0.4	2.18	2.0
–	2.42	5.4

EXAFS data in general agree with these results, giving further structural details. Thus, as follows from Fig. 3, even in pure ceria prepared by Pechini method and annealed at 700 °C, a peak at ~2.3 Å corresponding to the first Me–O distance is strongly asymmetric. Hence, oxygen polyhedra are strongly distorted, apparently due to residual lattice hydroxyls. This distortion is decreased for samples with a low dopant content, which can be assigned to the structure relaxation due to appearance of anion vacancies. However, at a high dopant content, it increases again, while intensity of all peaks declines due to structure disordering. Some peaks are even shifted and split thus indicating on the structure rearrangement. Similarly, coordination sphere of Sm cations is distorted as well. Since positions of Me–O peaks are identical for Ce and Sm spectra, this implies that Sm is indeed located in the regular sites of ceria lattice.

For Bi-doped samples asymmetric oxygen environment around cations and differing cation–cation distances are observed as well (spectra are not shown for brevity). Thus, for Ce cations two distances Ce–O ~2.2 and 2.4 Å with CN ~3.0 and 5.6 were revealed. The same is true for the Me-Me distances: Ce–Bi (R ~3.81–3.85 Å; CN ~2.9–3.6) and Ce–Ce (R ~3.80–3.85 Å; CN ~2.7–3.5).

Hence, a local structure of those apparently cubic solid solutions is strongly tetragonally distorted. What is different from the Ce–Sm system is that a local coordination of Bi

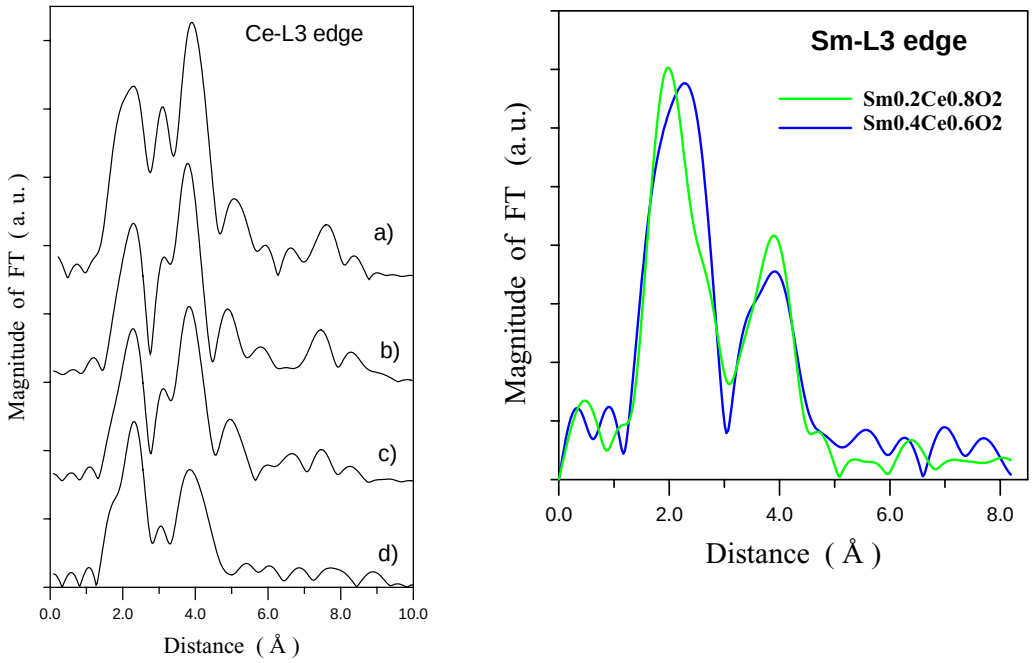

Fig. 3. EXAFS radial distribution function curves describing Ce and Sm local arrangement for $Sm_xCe_{(1-x)}O_2$ samples calcined at 700 °C: left part – Ce-L3 edge (a) CeO_2; (b) $x = 0.1$; (c) $x = 0.2$; (d) $x = 0.4$; right part – Sm-L3 edge.

cations differs from that of Ce, Me–O distances are shorter and coordination numbers are lower (*R* Bi–O ~2.00–2.21 Å; CN ~1.7–2.4) being close to that in the cubic δ-Bi_2O_3 phase. This implies that anion vacancies are mainly located in the coordination sphere of Bi cations. Hence, diffusion paths in the lattice can consist in the oxygen anions jumping from the vicinity of Ce cation into the vacant position near a Bi cation.

The infra-red spectroscopy revealed splitting of bands corresponding to Me–O modes due to distortion of coordination polyhedra: apparent maxima are observed in the 310–500 cm^{-1} range for Ce–Bi–O system and at 350–515 cm^{-1} for Ce–Sm–O one. More apparent distortion was observed at a higher doping level, which agrees with a trend for a higher disordering for heavy-doped samples revealed by RED and EXAFS. Disordering is also reflected in decline of the Raman band intensity with a dopant content (Fig. 4) and appearance of low intensity side bands. Bands positions and decline of their intensity at disordering are similar to those earlier described in details for locally tetragonally distorted Ce–Zr–La(Y)–O system [18]. However, for Ce–Sm–O system at the highest doping level, the intensity increases again due to a local rearrangement of the structure into that of a lower symmetry.

As follows from the DRS spectra (Fig. 5), absorption in the visible range corresponding to Ce^{3+} cations goes through the maximum at a low substitution degree correlating with the density of free (isolated) vacancies.

3.2. Surface properties

For pure ceria prepared via Pechini route, only weak Lewis acid sites-coordinatively unsaturated Ce^{3+} and Ce^{4+}

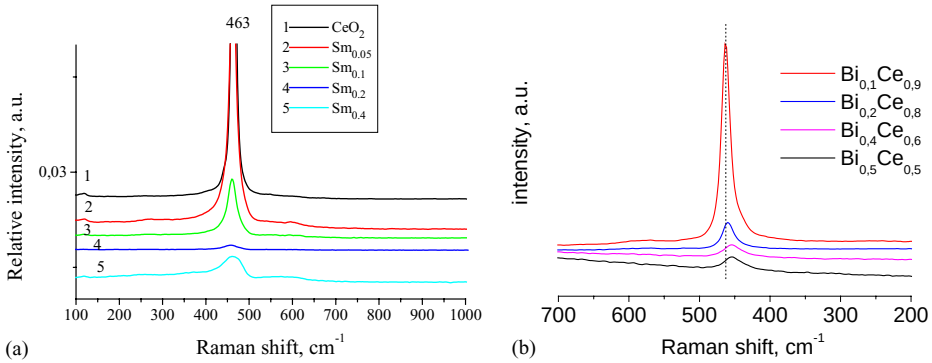

Fig. 4. Raman spectra for calcined at 500 °C ceria samples doped with Sm (a) and Bi (b).

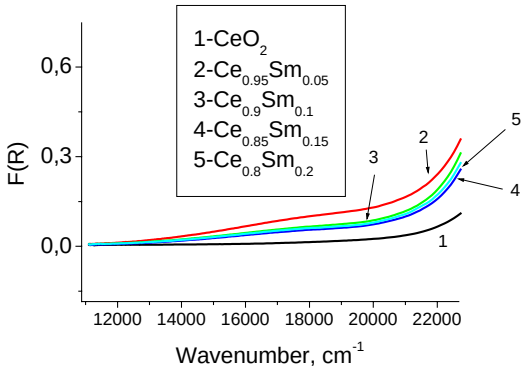

Fig. 5. Diffuse reflectance spectra of Sm-doped ceria samples (calcined at 700 °C) in the visible range.

cations (bands at ~2110–2120 and 2160–2180 cm^{-1}) are observed at 77 K (Fig. 6). Much lower intensity of Me^{3+}–CO bands suggests much lower surface concentration of corresponding adsorption sites. The increase of CO coverage shifts the maximum of Me^{4+}–CO bands to lower frequencies, while position of their right-hand slope remains unchanged. This is a typical feature of isolated centers slightly differing by their strength [19]. These sites are assigned to seven-coordinated Ce^{4+} cations located at the most developed (1 1 1) plane of fluorite-like oxides [19]. Due to only electrostatic type of interaction between CO and those centers, the band position (ν_{CO}) is determined by the effective charge of these cations, which primarily depends upon the number of oxygen anions in their coordination sphere. Besides, in the presence of gas-phase CO, a band at ~2144 cm^{-1} corresponding to CO bound with weakly acidic bridging surface hydroxyls is well developed.

Terminal hydroxyls are absent, and bridging hydroxyls weak Broensted acid sites are represented by bands in the 3570–3644 cm^{-1} region.

The surface density of Lewis and Broensted acid sites related per the unit surface area was found to go through the maximum with Sm content, as illustrated in Fig. 6 for complex oxides both pure and promoted by Pt. This means that the density of surface defects coordinatively unsaturated Ce^{4+} cations correlates primarily with the density of free (isolated) anion vacancies and not with the density of domain boundaries (vide supra). Since these sites are isolated, rearrangement of the ceria structure with the dopant content affects only slightly their coordination sphere (hence, effective charge, and, as the result, carbonyl band position), being reflected only in their density (intensity of Me^{4+}–CO band). More subtle and complex changes with the dopant content in the intensity and position of Me^{3+}–CO band (probably associated with clustered centers [2,19]) are beyond the scope of this paper and will be presented elsewhere.

The intensity of Pt–CO band correlates with the density of support acid sites, implying their role in anchoring Pt clusters, thus helping to increase their dispersion. For comparison, the data for Pt supported onto another type of fluorite-like solid solution, ceria–zirconia system [2,3] are presented as well. The latter system possesses a higher density of the surface acid sites due to a stronger distortion of the oxygen polyhedra by small Zr cations [2,3,18]. Moreover, for Zr-containing samples, the right-hand slope of Me^{4+}–CO adsorption band is blue-shifted, thus indicating on the presence of coordinatively unsaturated Zr^{4+} cations with a higher effective charge [19]. However, in general, the intensity of bands corresponding to Pt–CO complexes is comparable for both systems. Hence, the chemistry of the surface, namely, interaction of acid H_2PtCl_6 with basic surface sites (oxygen anions or basic La cations) at the impregnation stage is to be taken into account as well, which requires further studies.

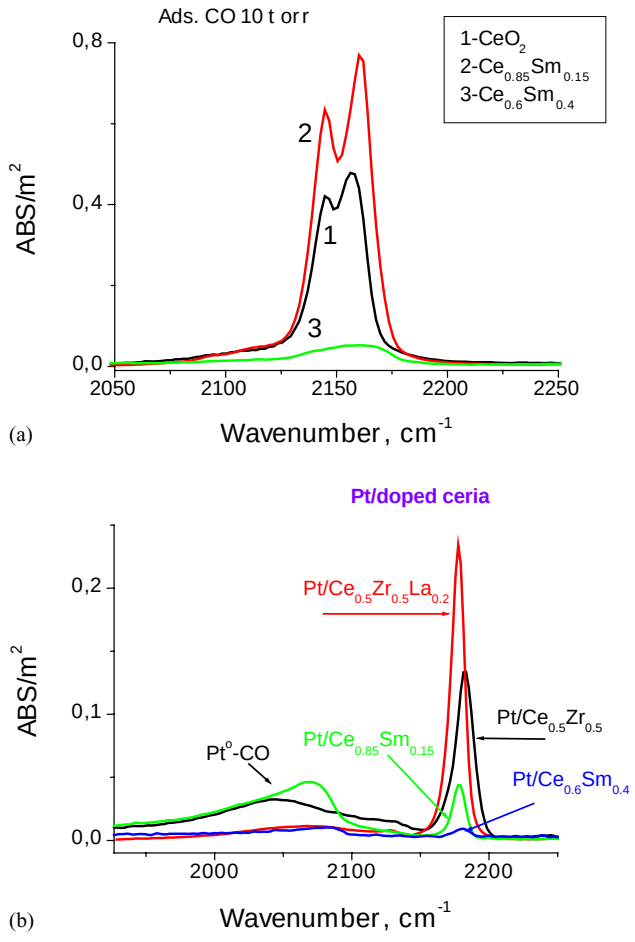

Fig. 6. FTIRS spectra of CO adsorbed at 77 K on pretreated in vacuum at 400 °C samples: (a) ceria and Sm-doped ceria samples, PCO = 10 Torr; (b) Pt-supported Ce–Sm and Ce–Zr (La) samples, 16 μmol CO is adsorbed.

3.3. Oxygen isotope exchange

The oxygen heteroexchange on fluorite-like systems corresponds mainly to the 3rd type, i.e. with participation of two surface oxygen atoms [9]. Activation energy was estimated to be ~80 kJ/mol, reaction order in the studied pressure range (100–300 Pa) ~0.5.

Table 2
Oxygen isotope exchange on fluorite-like oxides

Sample	T (K)	P (Pa)	X_e [a]	$R/10^{15}$, O_2 (m^2s)[b]
$Sm_{0.2}Ce_{0.8}O_{1.9}$	723	140	7	1.4
$Ce_{0.5}Zr_{0.5}O_2$	773	140	1	1.5
$Pt/Ce_{0.5}Zr_{0.5}O_2$	773	110	7	2.4

[a] Amount of exchangeable oxygen, in monolayers.
[b] Rate of heteroexchange at the experimental pressure.

In dynamic experiments [9], i.e. when the oxygen exchange is carried out in the temperature-programmed regime, the amount of exchangeable oxygen (X_e) for the Ce–Sm–O system was found to go through the maximum ($X_e \sim 2$ monolayers) at a relatively low substitution degree ($x = 0.2$) correlating with the density of isolated anion vacancies. Though ceria–zirconia system possesses a higher density of the surface Me^{4+} defects (vide supra), the rate of the oxygen exchange as well as the amount of exchangeable oxygen were found to be lower (Table 2). All these data are in favor of the heteroexchange reaction being controlled by the density of anion vacancies in the lattice (bulk mobility) and not by the surface steps [9]. In agreement with this suggestion, Pt supporting on Ce–Zr–O system has only a little effect on the rate of exchange but somewhat increases the amount of exchangeable oxygen. This feature can be assigned to Pt incorporation into the surface layer leading to activation of the oxygen atoms [7].

3.4. Hydrogen TPR

In hydrogen temperature-programmed reduction (TPR), incorporation of Sm into ceria increases reactivity in the middle-temperature (~500 °C) range, apparently due to appearance of anion vacancies in the lattice (Fig. 7). The most reactive forms removed by H_2 at ~250 °C appear to be located at the surface defects created by Sm incorporation. The overall amount of oxygen removed from these samples by hydrogen in TPR run (~1 monolayer) is less than required for reduction of all Ce^{4+} cations to Ce^{3+} state. Hence, this amount is controlled by kinetic factors. The decline of domain size and increase of the domain boundaries density with x (vide supra) has not caused any pronounced effect on the 1st peak position (mainly, the surface and subsurface layer reduction), while moving the 2nd one (bulk reduction) to lower temperatures and decreasing its intensity. This implies that in our case domain boundaries are at least not barriers for the oxygen diffusion in the lattice. Decline of the relative reactivity of sample with the highest Sm doping level seems to correlate with decline of the density of bulk and surface vacancies caused by the structure rearrangement (vide supra). Pt supporting shifts the TPR peak to lower temperatures due to more efficient hydrogen activation. Moreover, the effect of the samples composition on the amount of removed oxygen (only slightly increased due to Pt addition) becomes less apparent, which agrees with

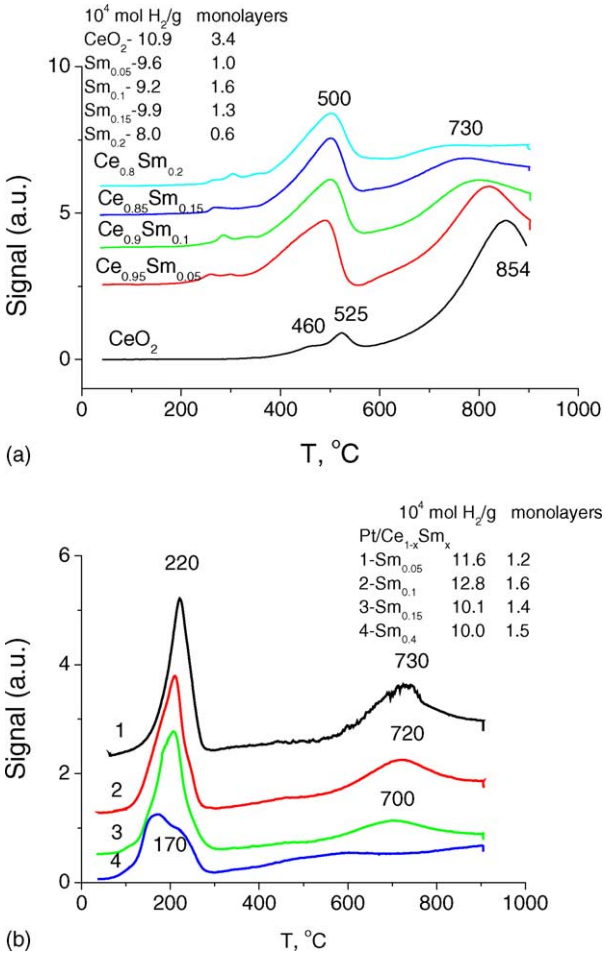

Fig. 7. H_2 TPR for samples of ceria–samaria system pretreated in O_2 at 500 °C for 1 h: (a) pure supports; (b) with supported Pt.

suggestion that reduction of those oxides by hydrogen is at least in part controlled by the surface stages.

For Bi-doped ceria samples even without Pt, H_2 TPR peaks are shifted to lower temperatures ($T_{max} \sim 300$ °C, a shoulder at ~220 °C, positions not sensitive to Bi content) as compared with Sm-doped samples (TPR curves not shown for brevity). Only a small part of oxygen is removed at higher temperatures, thus demonstrating efficient bulk reduction of these samples. The overall amount of removed oxygen increases with substitution due to Bi cations reduction into metal. For this system, a negative effect of domain boundaries was not observed as well. Hence, low-coordinated Bi cations appear to very efficiently activate hydrogen molecules. Pt addition even somewhat shifts reduction to higher temperature ($T_{max} \sim$ 330–340 °C, shoulder at ~230–240 °C), probably due to a partial shielding of the surface Bi cations. Moreover, TPR maxima are shifted to higher temperatures as compared with supported Pt/Ce–Sm samples (cf. Fig. 7). Hence, Pt is somewhat deactivated due to interaction with Bi. Here, combination of Pt and Bi has brought no advantages due to poisoning effect of Bi in cationic or metallic state on the surface of Pt particles.

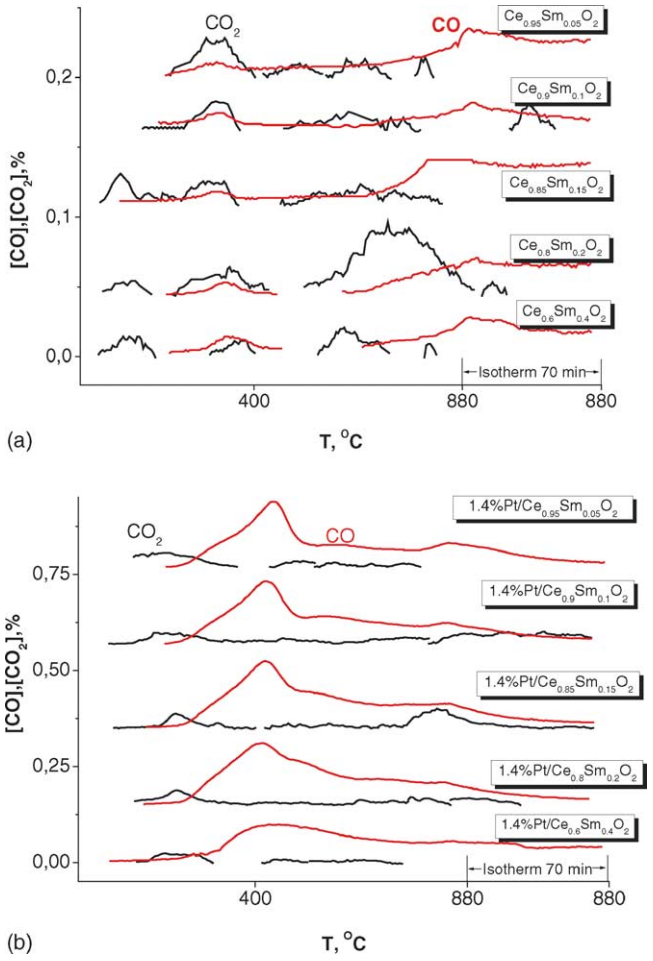

Fig. 8. Typical CH_4 TPR curves (1% CH_4 in He, heating rate 10°/min) for samples of ceria–samaria system pretreated in O_2 at 500 °C for 1 h: (a) pure supports; (b) with supported Pt.

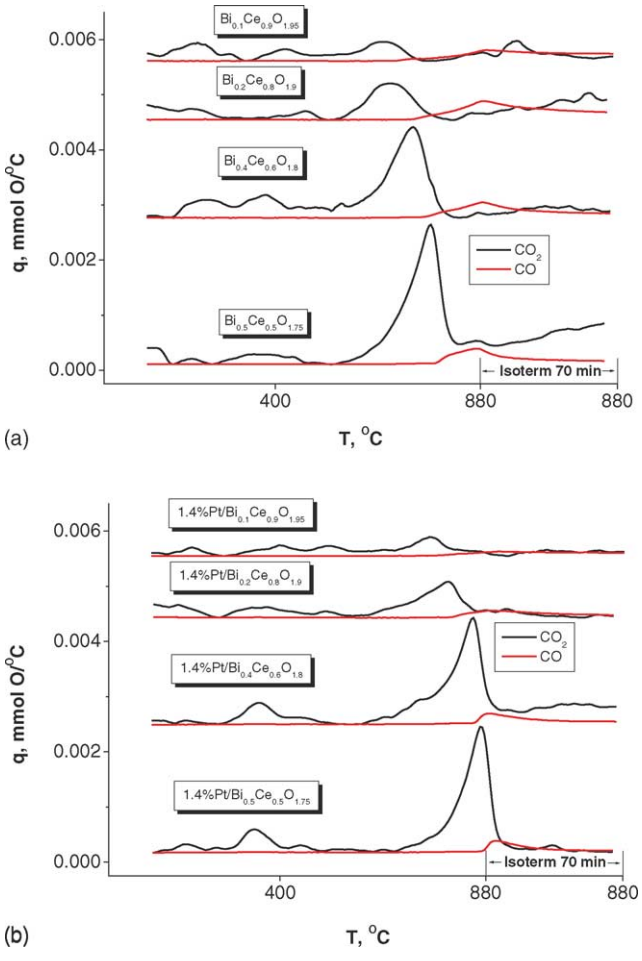

Fig. 9. Typical CH_4 TPR curves (1% CH_4 in He, heating rate 10°/min) for samples of Bi-doped ceria samples pretreated in O_2 at 500 °C for 1 h: (a) pure supports; (b) with supported Pt.

3.5. Methane TPR

In the reaction of TPR by methane, for Ce–Sm–O samples, the most reactive oxygen forms are mainly removed at low temperatures giving deep oxidation products, while syngas is mainly produced at higher temperatures (Fig. 8). This is a rather general phenomenon, since similar features were revealed in CH_4 TPR for Sr-substituted lanthanum ferrites [20]. Even without supported Pt, Ce–Sm samples, especially those with a relatively low (∼0.2) doping level, are reasonably efficient in syngas generation. This correlates with the amount of isolated anion vacancies and surface defects reaching a maximum in this doping range. At a higher Sm content a structure rearrangement is reflected in the high-temperature CO_2 peak and/or in decline of syngas yield in the isothermal part of run.

For Sm-doped system Pt addition shifts reduction to lower temperatures and improves syngas selectivity. Peaks of CO_2 and H_2O evolution were found to coincide, and no water was produced at T_{max} of CO peak, hence, only syngas was generated in this range. Some coke in a small amount (not exceeding 1% of converted methane) is deposited on the surface yielding CO_2 and H_2O at reoxidation. The highest performance is revealed for samples with a moderate doping level possessing the highest oxygen mobility as well as the highest metallic Pt dispersion, though the scale of effect is small. Much stronger reduction was achieved with methane as reducing agent as compared with hydrogen (all Ce cations are reduced to 3+ state), which agrees with the same trend observed in [20] for ferrites.

For Bi-doped system both with Pt or without it, mainly deep oxidation products are observed (Fig. 9). This apparently correlates with the well-known ability of Bi cations to activate hydrocarbons yielding radicals. As was revealed earlier, bismuth-based cubic solid solutions doped by Y and Sm are not reduced by methane at all, while being completely reduced by H_2 in a narrow peak with $T_{max} \sim 360$–390 °C [21]. Hence, ceria matrix is responsible for such enhanced activity of Bi cations towards methane, probably making them more coordinatively unsaturated (vide supra). From the practical point of view, Ce–Bi–O electrolytes should not contact methane being used only at the air side of a membrane.

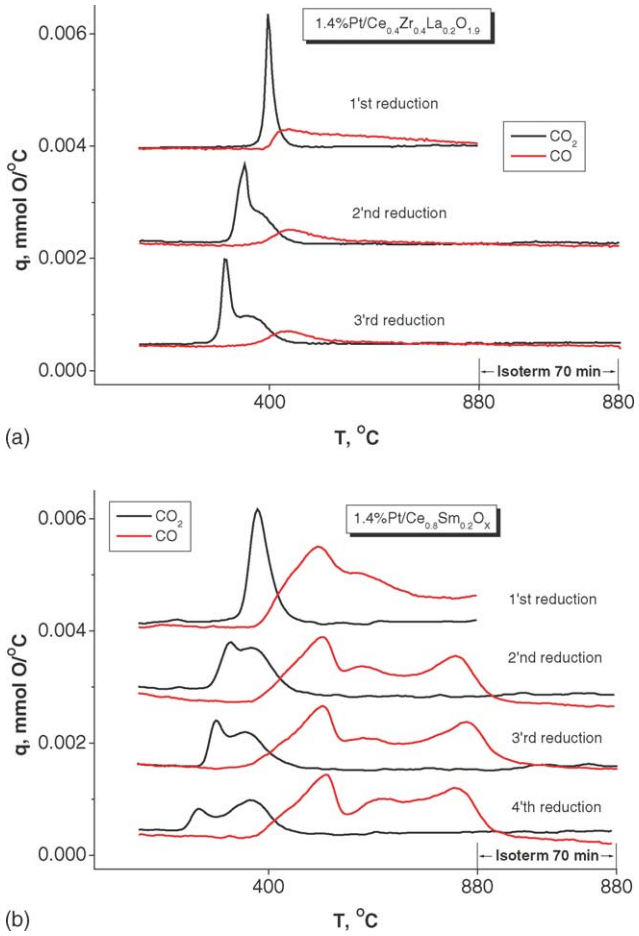

Fig. 10. Typical curves of the lattice oxygen consumption for deep oxidation products (CO_2) and syngas (CO) as dependent upon the number of redox cycles: (a) Pt/Ce–Zr–La–O; (b) Pt/Ce–Sm–O. Samples are reoxidized at 500 °C up to saturation first in the flow of 1% O_2 in He, then in 20% O_2 in He.

For another fluorite-like solid solution based upon ceria–zirconia system, which is also considered to be promising for the practical application as an active component of catalysts for methane selective oxidation into syngas, a bigger part of the lattice oxygen is consumed for the methane deep oxidation (Fig. 10). This is not expected since the lattice oxygen mobility for this system is lower than that for Ce–Sm–O (vide supra). However, this behavior seems to correlate with a higher density of the surface defects (vide supra). Hence, even when the surface of mixed oxide catalyst is promoted by Pt known for its high efficiency in the methane activation, and even in the absence of gas-phase oxygen, the nature of the support surface acid sites apparently affects the route of methane transformation. Moreover, for Ce–Zr–O system in a cyclic redox process (Fig. 10), its apparent activation due to mild reoxidation conditions [22], shifts reduction to lower temperatures decreasing the yield of syngas. In contrary, for Ce–Sm–O system performance and syngas selectivity are not deteriorated after numerous cycles (Fig. 10). Moreover, for Zr-doped ceria a bigger amount of coke was deposited at the surface as revealed by oxidation after TPR run (not shown for brevity). Hence, at least for the cyclic process of syngas generation from methane, ceria–zirconia-based system is less promising as compared with the Ce–Sm one.

4. Conclusions

Comparison of three types of fluorite-like complex oxide systems made in this work allowed to conclude that the selectivity of methane transformation into syngas by the lattice oxygen depends not only on the route of its primary activation (i.e. on supported Pt clusters) but on the features of activated fragments transformation on the support surface as well, provided the lattice oxygen mobility is comparable. Too high density of Lewis acid sites seems to favor deep oxidation of methane. From the point of view of those nanodomain systems performance, at least in reducing conditions, any negative effect of domain boundaries on the lattice oxygen mobility was not observed. A disordering of domain boundaries facilitating the oxygen transfer along and across those extended defects could be responsible for this phenomenon.

Ce–Sm-based fluorite-like oxide system promoted by Pt is promising for methane selective oxidation into syngas by the lattice oxygen due to a high mobility and reactivity of this oxygen, good selectivity for syngas and stability of performance in redox cycles. The bulk and surface structural features of samples of this system depends upon the Sm content due to the lattice rearrangement caused by dopant. The highest performance appears to be demonstrated by samples where isolated oxygen vacancies dominate. Pt/Ce–Zr–La–O system is less stable and selective in redox cycles and less active due to a lower lattice oxygen mobility and a higher density of surface defects. Bi–Ce–O system can be used only as a good mixed ionic–electronic conductor at the air side of membrane.

Acknowledgements

This work was in part supported by International Projects INTAS – 01-2162, ISTC 2529 and Integration Projects 39 and 110 SB RAS.

References

[1] M.P. Pechini, US Patent 3, 330, 1967, 697.
[2] T.G. Kuznetsova, V.A. Sadykov, E.M. Moroz, S.N. Trukhan, E.A. Paukshtis, V.N. Kolomiichuk, E.B. Burgina, V.I. Zaikovskii, M.A. Fedotov, V.V. Lunin, E. Kemnitz, Stud. Surf. Sci. Catal. 143 (2002) 659.
[3] T.G. Kuznetsova, V.A. Sadykov, S.A. Veniaminov, G.M. Alikina, E.A. Paukshtis, Ya.N. Kulikova, E.M. Moroz, E.B. Burgina, V.A. Rogov, V.N. Kolomiichuk, V.V. Kriventsov, D.I. Kochubei, O.N. Martyanov,

V.F. Yudanov, I.S. Abornev, S. Neophytides, ISO22, Europacat VI, September 2003, Innsbruck, Austria.
[4] J. Zaman, A. Chakma, J. Membr. Sci. 92 (1994) 1.
[5] K. Otsuka, E. Sunada, T. Ushiyama, I. Yamanaka, Stud. Surf. Sci. Catal. 107 (1997) 531.
[6] L.V. Mattos, E.R. de Oliveira, P.D. Resende, F.B. Noronha, F.B. Passos, Catal. Today 77 (2002) 245.
[7] V.A. Sadykov, T.G. Kuznetsova, S.A. Veniaminov, V.V. Lunin, E. Kemnitz, A. Aboukais, React. Kinet. Catal. Lett. 76 (2002) 83.
[8] V.A. Sadykov, T.G. Kuznetsova, V.P. Doronin, T.P. Sorokina, D.I. Kochubei, B.N. Novgorodov, V.N. Kolomiichuk, E.M. Moroz, D.A. Zyuzin, E.A. Paukshtis, V.B. Fenelonov, A.Ya. Derevyankin, S.A. Beloshapkin, V.A. Matyshak, G.A. Konin, J.R.H. Ross, Mat. Res. Soc. Symp. Proc. 703 (2002) 529.
[9] V.S. Muzykantov, V.A. Sadykov, E. Kemnitz, V.V. Lunin, Kinet. Katal. 44 (2003) 349.
[10] G. Li, Y. Mao, L. Li, Sh. Feng, M. Wang, X. Yao, Chem. Mater. 11 (1999) 1259.
[11] S. Dickmen, P. Shuk, M. Greenblatt, Solid State Ionics 112 (1998) 299.
[12] Y. Ito, Y. Lei, N.D. Browning, T.J. Mazanec, Mat. Res. Soc. Symp. Proc. 703 (2002) 489.
[13] H. Inaba, H. Tagawa, Solid State Ionics 83 (1996) 1.
[14] J.-H. Hwang, T.O. Mason, Z. Phys. Chem. 207 (1998) 21.
[15] P. Knauth, H.L. Tuller, Mat. Res. Soc. Symp. Proc. 548 (1999) 429.
[16] S. Yamazaki, T. Matsui, T. Ohashi, Y. Arita, Solid State Ionics 136-137 (2000) 913.
[17] D.A. Zyuzin, E.M. Moroz, V.A. Sadykov, T.G. Kuznetsova, A.N. Shmakov, Izv. Ras, Ser. Phiz. 68 (2004) 732.
[18] L.N. Ikryannikova, A.A. Aksenov, G.L. Markaryan, G.P. Murav'eva, B.G. Kostyuk, A.N. Kharlanov, E.V. Lunina, Appl. Catal. A 210 (2001) 225.
[19] K.I. Hadjiivanov, T.N. Vaysillov, Adv. Catal. 47 (2002) 307.
[20] R. Li, Ch. Yu, Sh. Chen, J. Natl. Gas Chem. 11 (2002) 137.
[21] V.V. Zyryanov, N.F. Uvarov, V.G. Kostrovskii, V.A. Sadykov, T.G. Kuznetsova, V.A. Rogov, V.I. Zaikovskii, Y.V. Frolova, G.M. Alikina, G.S. Litvak, E.B. Burgina, E.M. Moroz, S. Neophytides, Mat. Res. Soc. Proc. 755 (2003) DD6.27.
[22] G. Balducci, P. Fornasiero, R. Di Monte, J. Kaspar, S. Meriani, M. Graziani, Catal. Lett. 33 (1995) 193.